Switching of photocurrent polarity in electrochemical cells with light via an excited state proton transfer mechanism

Anna Yuchnovsky[1,a], Yaniv Shlosberg[1,2a], Noam Adir[1,2], and Nadav Amdursky[1,2*]

[1] Schulich Faculty of Chemistry, Technion – Israel Institute of Technology, Haifa 32000, Israel

[2] Grand Technion Energy Program, Technion – Israel Institute of Technology, Haifa 32000, Israel

[a]Equal contribution

*Corresponding author: amdursky@technion.ac.il

Abstract

Light is the most targeted source of energy for sustainable energy technologies such as in photocurrent generation. While practically all light-harvesting types of applications utilize the electrons in their excited state (ES), here, we introduce a new conceptual approach that is based on ES proton transfer (ESPT). We use Brønsted photoacids and photobases that can donate or accept a proton, respectively, but only in their ES. Here, we use these molecules solvated in a photoelectrochemical single cell and explore the role of ESPT in photocurrent generation. We show at different bias regimes that the formed ions following the ESPT process can serve as electron donors or acceptors to the electrodes, which is dependent on the system and the presence of a photoacid or a photobase, resulting in modulating the photocurrent generation toward positive or negative currents. We further use an H-cell configuration that allows us to control the current polarity by switching the illumination between the cell containing the photoacid to the one containing the photobase. Our study represents a new approach in photoelectrochemistry by introducing ESPT processes, which can be further utilized in future devices targeting light-responsive energy production, energy storage, and hydrogen formation applications.

Keywords: Photoacids, Photobases, Electrochemical cell, 2-naphthol-6-sulfonate, 6-aminoquinoline.

Introduction

The road to sustainable clean energy technologies is of prime importance to our planet, whereas light is the most targeted sustainable source of energy. Among the different light-harvesting technologies, we will focus here on photoelectrochemistry. Photoelectrochemical cells are usually designed to either generate hydrogen by electrolysis or to generate photocurrent, i.e., they can be analogous to photovoltaic cells,[1-3] such as dye-sensitized photoelectrochemical cells that make use of light-sensitive organic dyes (photosensitizers) for photocurrent generation.[4-7] Other common applications of photoelectrochemical cells are taking advantage of the photocurrent polarity for sensing and logical operation.[8-10]

An important parameter in electrochemical processes is their dependence on the local pH,[11-17] meaning the local concentration of protons next to the electrode. Here, we use unique molecules that can manipulate the proton concentration using light as an energy source. Specifically, we are using Brønsted photoacids (PAs) and photobases (PBs) that become strong acids and bases only as a response to light absorption. This property of PAs and PBs is due to their fundamental change in pK_a that drops or rises, respectively, upon excitation, thus resulting in an excited state proton transfer (ESPT) event.[18-21] Therefore, in their electronically excited state, a PA dissociates and transfers the proton to a proton acceptor, such as water or another solvated molecule, while a PB acts in a reverse mode by abstracting a proton from a proton donor, which similarly can be water or another donor. This ability of Brønsted PAs and PBs has been used before to dynamically control dynamic processes that are dependent on the protonation or deprotonation of molecules, such as self-assembly processes, enzymatic activities, self-propulsion, and protonic transport.[22-29] It is worth mentioning that other types of molecules are also termed PAs, which are not Brønsted type, but rather a photochromic molecule that undergoes a light-induced structural change in which a proton is released, with the spiropyran-merocyanine system being the common representative of photochromic PAs. Whereas photochromic PAs can induce a transient change of the pH, Brønsted PAs do not induce a change of the pH but they can undergo ESPT to a certain proton acceptor.

In this work, we show a new application of Brønsted PAs and PBs for light-driven photoelectrochemical photocurrent generation. We demonstrate that the ESPT of PAs and PBs can be utilized for photocurrent production and polarity switching in an electrochemical cell, both in single-cell and H-cell configurations. Unlike common photoelectrochemical devices for photocurrent generation, the use of PAs and PBs results in a fundamentally different

mechanism for photocurrent generation. In common photoelectrochemical cells, photocurrent generation is a resultant of an electron transfer process between the electronically excited state and the electrode. In the devices presented here, the photocurrent generation is due to an ESPT process. The new concept presented in this work can result in a new generation of future photoelectrochemical cells, either for photocurrent generation or hydrogen generation.

Results and Discussion

Spectroscopic characterization of the ESPT process

In this study, we have chosen the common 2-naphthol-6-sulfonate (2N6S) as the PA and 6-aminoquinoline (6AQ) as the PB (**Figure 1a**). The hallmark of the ESPT process is the deprotonation of the PA (ROH) to RO^- and the protonation of the PB (RN) to RNH^+ only upon light excitation, which is due to the different pK_a values between the ground and excited states (**Figure 1a**). The ESPT process can be observed spectroscopically since the protonated and deprotonated states of both the PA and the PB absorb and emit at different wavelengths. Indeed, while the UV-Vis ground state absorption spectra of 2N6S and 6AQshow that 2N6S is in its ROH state and 6AQ is in its RN state (**Figure 1b**, black curves), the emission spectra, that probe the excited state, show that 2N6S is in its RO^{-*} state and 6AQ is in its RNH^{+*} state (**Figure 1b**, red curves). Importantly, the emergence of the ionic forms following PA and PB excitation is only in the excited state with time scales of a few nanoseconds. Thus, upon returning to the ground state, the ESPT will be followed by a fast recombination process that will result in the molecules returning to their initial ROH/RN states.

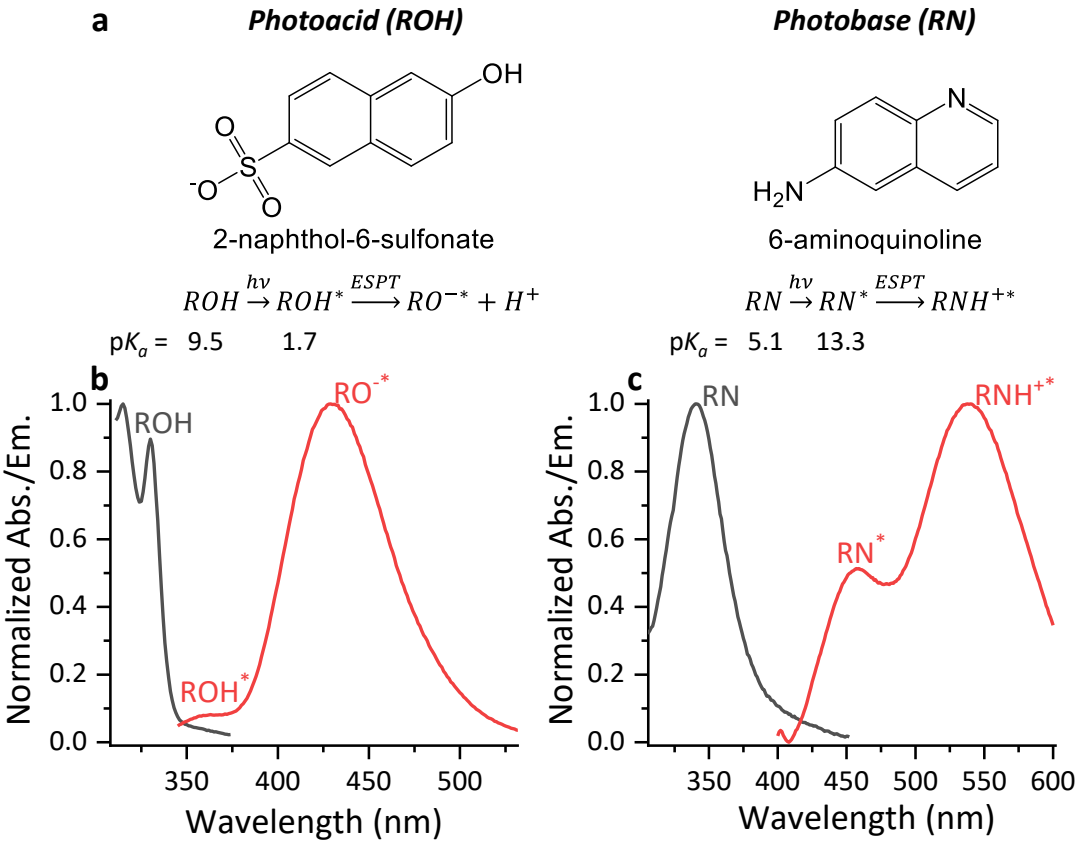

Figure 1. ESPT reactions by the 2N6S PA and the 6AQ PB. (**a**) molecular structures and reactions of 2N6S (ROH) and 6AQ (RN), showing also the pK_a change between ground and excited states. (**b**) and (**c**) Absorption (black curves) and emission (red curves) spectrum of 2N6S and 6AQ, respectively. λ_{ex}=340 nm for the emission spectra.

Photocurrent production of 2N6S at negative potential bias

In the first part of our study, we used a photoelectrochemical cell composed of a single cell setup using a screen-printed electrode with a graphite working electrode (WE), platinum counter electrode (CE), and silver coated with a silver chloride reference electrode (RE). To study the photoelectrochemical properties of 2N6S we performed cyclic voltammetry (CV) in dark and under UV irradiation using a LED with λ_{ex}=340 nm (**Figure 2a**). We observed that only under irradiation a positive peak with a maximum at 0.5 V, and a negative peak at -0.5 V were formed. As none of these peaks appeared in the dark measurements, or in measurements of pure electrolyte (**Figure S1**), it implies that these peaks are from the formation of the ionic forms: RO^- and H^+. While H^+ can only accept electrons, we ascribed it to the new peak at -0.5

V, while the peak at 0.5 V can be ascribed to the RO^-. In this section, we will focus on the negative bias regime. Following the reduction peak at the negative bias of -0.5 V (i.e., at biases lower than -0.5 V), the absolute current under light irradiation was about 0.5 µA lower (i.e., less negative) than in dark. Accordingly, we chose to work at this negative bias regime, where we decided to apply -1 V. It is important to note here that in the location of the reduction peak at -0.5 V, the current magnitude between light and dark was nearly identical. As will be described below, at the positive bias regime we could have used the exact location of the oxidation peak at 0.5 V.

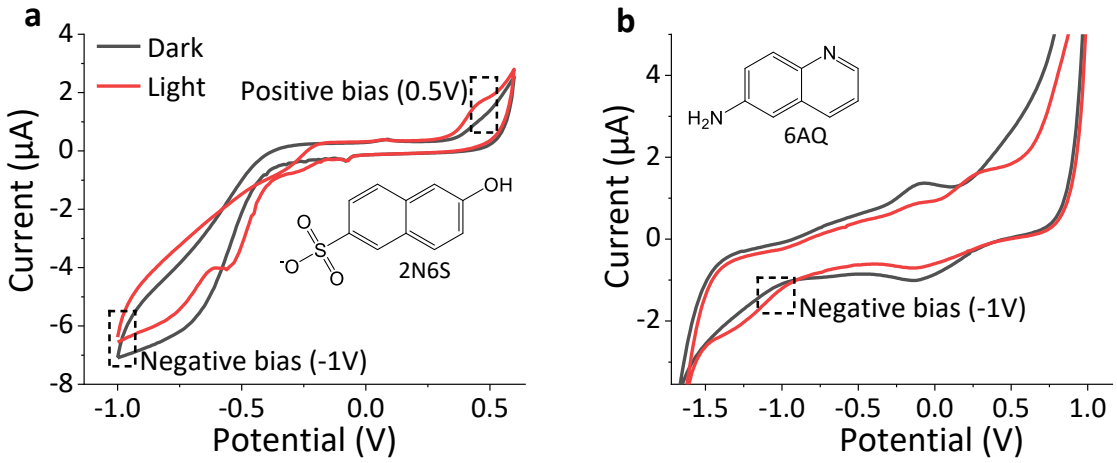

Figure 2. Cyclic voltammetry at dark and under light illumination (λ_{ex}=340 nm) of an aqueous solution containing (**a**) the 2N6S PA and (**b**) the 6AQ PB. The negative and positive bias regimes used below are marked in the figure by the dashed rectangles.

To follow photocurrent generation in this section, we measured the chronoamperometry (CA) of 2N6S under the application of a negative -1 V on the WE with dark/light irradiation intervals of 100 s (**Figure 3a**). The results clearly show a light response of the measured current, exhibiting a positive change in current density (i.e., lower absolute values) upon light irradiation with an absolute value of 0.97 ± 0.22 µA/cm^2. While turning off the light, the current density has returned to its initial value (prior to irradiation).

To explain our results, we need to turn to the energy scheme of the different electronic processes. As mentioned, we suggest here that at the negative bias regime, H^+ acts as an electron acceptor from the WE (**Figure 3b**). The application of a negative potential at the WE alters its energy level that becomes higher than the one of the CE (**Figure 3c**). Accordingly, the electron flow direction is now from the CE to the WE. Thus, we can postulate that the

increase in positive current density upon light irradiation is derived from the oxidation of the platinum CE by H^+ ions that were formed under irradiation (**Figure 3b**). To support our hypothesis here, we have conducted a control experiment, where the current was measured at the negative bias regime in the absence of PA in the solution, but in the presence of HCl in the electrolyte. In this control experiment, we observed an increase in the current density upon the addition of HCl (**Figure S2**). This important result supports our hypothesis that the positive current increase originates from the oxidation of the platinum CE by H^+ ions. As discussed above, the use of a Brønsted PA does not result in the acidification of the electrolyte, but rather, a direct 'scavenging' of the proton by the electrode occurs. To conclude, the working mechanism of the PA in the negative bias regime (**Figures 3b** and **3c**), our results suggest that before irradiation, water molecules serve as both electron donors to reduce the CE and electron acceptors to oxidize the WE, whereas the electrons flow from the CE towards the WE. Upon UV irradiation, the 2N6S PA deprotonates, and the generated protons serve as electron acceptors from the CE. This process is a competing reaction to the reduction of the CE, and accordingly, results in a positive current density increase.

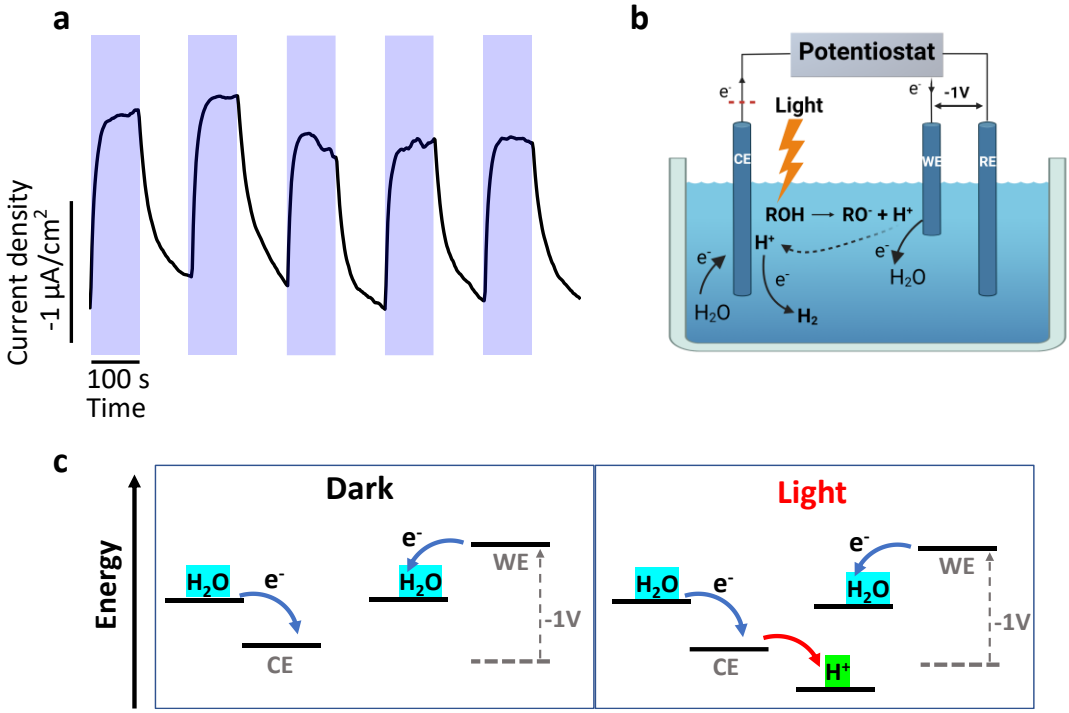

Figure 3. 2N6S PA on a printed electrode under -1V bias. (**a**) The changes in the measured CA upon light irradiation (λ_{ex}=340 nm) are marked with purple rectangles. (**b**) A schematic model of the system and (**c**) energy levels diagram of the system at this negative bias regime showing also the ESPT process and the flow of electrical current in the system.

Photocurrent production of 2N6S at positive potential bias

As discussed, our CV measurements of 2N6S showed the formation of a positive peak at around 0.5 V that was ascribed to the formation of RO^- (**Figure 2a**). Thus, to complement these results, we now turned to the positive bias regime, while applying a positive potential bias of 0.5 V on the WE. The CA measurements of 2N6S under dark/light irradiation intervals of 100 s (**Figure 4a**) showed that in the positive bias regime, irradiation of 2N6S resulted in an increase in the absolute current density of 0.07±0.02 $\mu A/cm^2$. As before, upon turning off the irradiation, the current density decreased back to the baseline level (prior to irradiation).

At a positive potential on the WE, the electrons flow from the WE to the CE. We suggest here that the increase in the positive current density can derive from the reduction of WE by the RO^- ions formed upon irradiation (**Figure 4b**). To support this hypothesis, and in line with the previous section, we conducted a control experiment where the electrolyte without the PA was titrated this time with the addition of RO^- (from an alkaline condition) during the measurement, which resulted in an increase of the current density (**Figure S3**). In addition, to refute the possibility that the increase in current density in the control experiment was due to the electrochemical activity of an alkaline solution, we titrated the electrolyte with NaOH, which resulted only in a negligible response (**Figure S3**). This result supports our initial suggestion that the positive current increase originates from the reduction of the WE by RO^- ions. Accordingly, we can conclude that in the dark, water molecules serve as both electron donors to reduce the WE and as electron acceptors for the CE (**Figure 4c**). Following UV irradiation, the PA (ROH) undergoes dissociation, and the formed RO^- ions donate electrons to the WE. To exclude the participation of the formed H^+ ions in the oxidation of CE in the positive bias regime for the photocurrent generation, we designed an additional control experiment where we titrated the electrolyte with HCl, resulting in a negligible effect at this positive bias regime (**Figure S4**), which is in contrast to the negative bias regime discussed above.

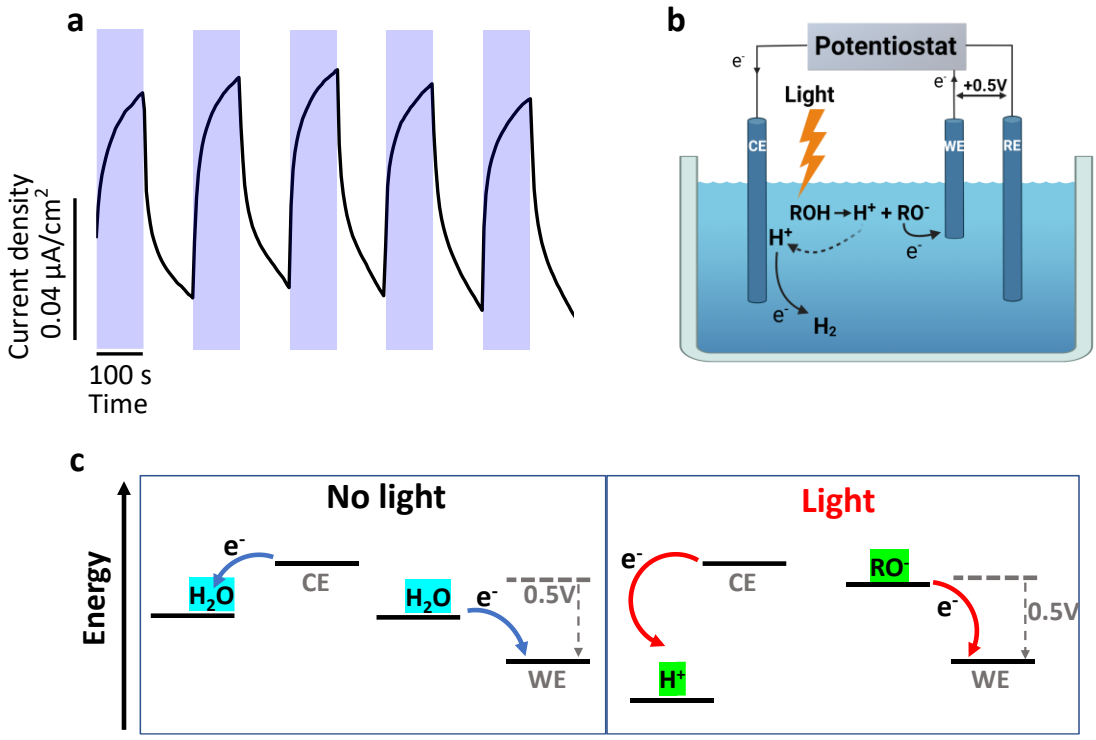

Figure 4. 2N6S PA on printed electrode under +0.5V bias. (**a**) The changes in the measured CA upon light irradiation (λ_{ex}=340 nm) are marked with purple rectangles. (**b**) A schematic model of the system and (**c**) energy levels diagram of the system at this negative bias regime showing also the ESPT process and the flow of electrical current in the system.

As discussed above, in most photocurrent generation types of devices, such as in electrochemical dye-sensitized solar cells, the photocurrent is obtained via direct electron (or hole) transfer between the photoexcited molecule in its higher energetic level and the electrode. In most cases, the photoexcited molecule forms a layer (either single or multi-layers) on the WE. In our system, we suggested a different mechanism for photocurrent generation that originates from a photo-dissociation reaction of the PA and an electrochemical reaction between the thus formed ions in the excited state and the electrodes. To support this mechanism, i.e., to exclude the direct electron transfer mechanism from the excited PA (ROH^*) to the electrode without the involvement of the ESPT process, we turned to the common PA of 8-hydroxypyrene-1,3,6-trisulfonic acid (HPTS), and its non-photoacid methylated analog, 8-methoxypyrene-1,3,6-trisulfonic acid (MPTS) (**Figure 5a**). We did not use the HPTS PA in the previous experiments due to its propensity to undergo bleaching upon prolonged exposure to light. In common with the 2N6S PA, HPTS also exhibits a predominately ROH peak in the absorption spectrum, at 405 nm, corresponding to the ground state form, and a predominant

RO^- peak in the emission spectrum, at 520 nm, corresponding to the excited state form (**Figure 5b**), which is due to the ESPT process. As opposed to this, the methylated form of HPTS (MPTS) exhibits only the $ROCH_3$ peak both in the absorption spectrum, at 405 nm, and in the emission spectrum, at 450 nm (**Figure 5c**). As MPTS is not dissociated by irradiation, any photocurrent generation would be possible only via a direct electron transfer mechanism. Thus, we followed the CA of HPTS and MPTS in dark/light irradiation (at λ_{ex}=405 nm) at intervals of 50 s with a similar applied positive potential of 0.5 V on the WE as was used above (**Figure 5d**). As shown in the figure, a maximal photocurrent production of 0.06 $\mu A/cm^2$ was obtained for HPTS following light irradiation, which decayed to the baseline level in dark, while no photocurrent production was detected for MPTS. In line with the CA results, the CV measurements also show that the CV response of MPTS is identical in both dark and light conditions, whereas HPTS shows a photocurrent generation upon light irradiation with 0.5V being the onset of the photocurrent (**Figure S5**). These results support our hypothesis that the photocurrent production from PAs derives from electrochemical reactions of the photo-dissociated ions in the excited state and not from a direct electron transfer to the electrode.

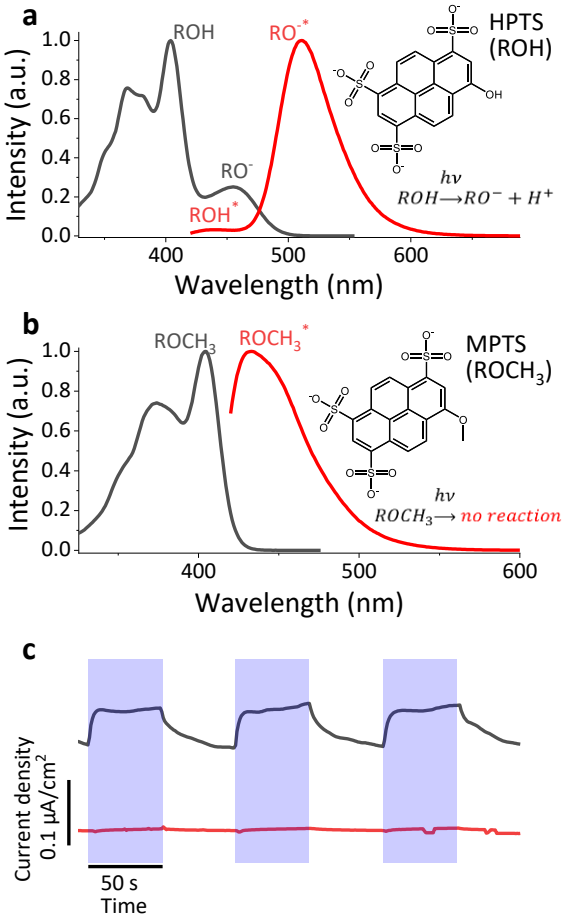

Figure 5. (**a**) and (**b**) Absorption (black curves) and emission (red curves) spectrum of HPTS and MPTS, respectively. λ_{ex}=405 nm for the emission spectra. The figures also show the

molecular structures and reactions of HPTS and MPTS. (**c**) The changes in the measured CA upon light irradiation (λ_{ex}=405 nm) are marked with purple rectangles of HPTS (black line) and MPTS (red line) under +0.5V bias.

Photocurrent production of 6AQ at negative potential bias

Here, we switch from having a PA in one cell configuration to having a PB in this configuration. As before, we first identified the electrochemical reactions of 6AQ PB by CV measurements in dark and under UV irradiation (**Figure 2b**). The unique electrochemical features that appear under light irradiation are a positive peak with a maximum around 0.4 V and a negative peak with a maximum around -1 V that are absent in the dark. Unlike the results obtained with the PA, here we focus only on the negative bias regime, which is due to similar currents at positive bias between dark and light around the oxidation peak at light conditions, after which, the very steep increase at higher biases (due to water electrolysis) has made the positive bias regime unfavorable for photocurrent production. Unlike the case of having a PA in the solution, here, having a PB resulted in a negative photocurrent upon the irradiation of 6AQ at the negative (-1V) bias regime (**Figure 6a**), where we observed an absolute measured photocurrent density of 0.05±0.01 μA/cm^2. Upon turning off the irradiation, the current density returned back to the baseline level. In line with our suggested hypothesis, in the dark, the PB behaves exactly as it was with the PA in the negative bias regime. However, under irradiation, the formed RNH^+ can now accept electrons from the WE (**Figures 6b** and **6c**). To support this hypothesis, we conducted a control experiment where we titrated the electrolyte with RNH^+ ions (from an acidic solution), which resulted in a decrease in the current (**Figure S6**). This result supports our hypothesis that the RNH^+ form is being reduced by the WE. As also shown in figure S6, a transient increase in currents was observed upon adding the RNH^+ ions prior to the decrease, which can be ascribed to the electrochemical activity of the acidic solution, similar to the HCl addition to the electrolyte (**Figure S2**).

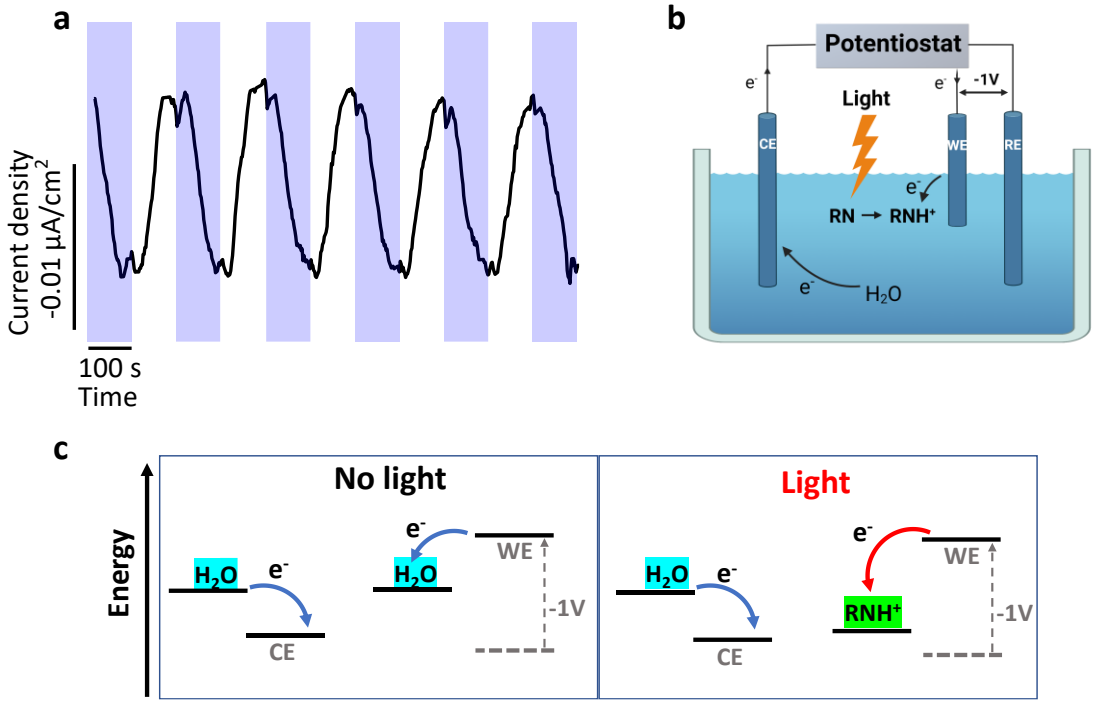

Figure 6. 6AQ PB on printed electrode under -1V bias. (**a**) The changes in the measured CA upon light irradiation (λ_{ex}=340 nm) are marked with purple rectangles. (**b**) A schematic model of the system and (**c**) energy levels diagram of the system at this negative bias regime showing also the ESPT process and the flow of electrical current in the system.

Switching current polarity by irradiation of 2N6S and 6AQ.

Until now, we have explored the photocurrent response of either a PA or a PB in a single cell configuration, showing that in the negative bias regime on the WE, a positive photocurrent is generated for the 2N6S PA (**Figure 3a**) and a negative photocurrent for the 6AQ PB (**Figure 6a**). As indicated in our suggested mechanisms, the photoelectrochemical reaction of 2N6S involves the reduction of H^+ ions into H_2 gas next to the platinum CE (**Figure 3b**), while the reaction of 6AQ involves the reduction of the formed RNH^+ by the WE (**Figure 6b**). In this section, we introduce a different design of a photoelectrochemical cell whose current polarity and hydrogen production can be photo-regulated. To this end, we designed an H-type cell made of glass with 2 quartz optical windows at the bottom of the WE and CE locations. In this way, we can irradiate each cell separately, whereas 2N6S was added to the half-cell containing a platinum CE, and 6AQ was added to a joint half-cell containing a graphite WE and an Ag/AgCl RE. To complete the setup, a proton conductive Nafion membrane was used to separate the two half cells (**Figure 7a** for the schematic of the H-cell). We used this setup to follow the CA at the negative (-1 V) bias regime on the WE (**Figure 7b**) while irradiating the different half

cells in the following sequence: irradiation of the 6AQ PB (100 s), dark (100 s), irradiation of the 2N6S PA (100 s), and dark (100 s). As seen in the figure, upon irradiation of 6AQ, a negative photocurrent was obtained, and by turning off the light, a positive current trend was obtained that brought the current close to its initial value. Following the latter, irradiation of 2N6S has inflicted a further positive photocurrent, which has decreased back to the initial baseline level upon turning off the light. Such photocurrent polarity trend upon irradiation of either 2N6S or 6AQ in the H-cell configuration is in line with the results obtained in the single-cell configuration. In terms of photocurrent magnitude, in the H-cell configuration, we received a negative photocurrent of ~40 $\mu A/cm^2$ upon the excitation of the PB and a positive photocurrent of ~20 $\mu A/cm^2$ upon the excitation of the PA. It is also important to note here the different kinetics of the photocurrent generation between the measurements in the single- and the H-cell- configurations. Whereas the photocurrent reaction lifetime in the PB was nearly identical between the two configurations, the one of the PA was nearly an order of magnitude slower in the H-cell configuration compared to the single-cell (**Table S1**). The reason for the large difference in the PA kinetics is due to the necessity of the protons to pass through the proton exchange membrane, which leads us to the final part of our study.

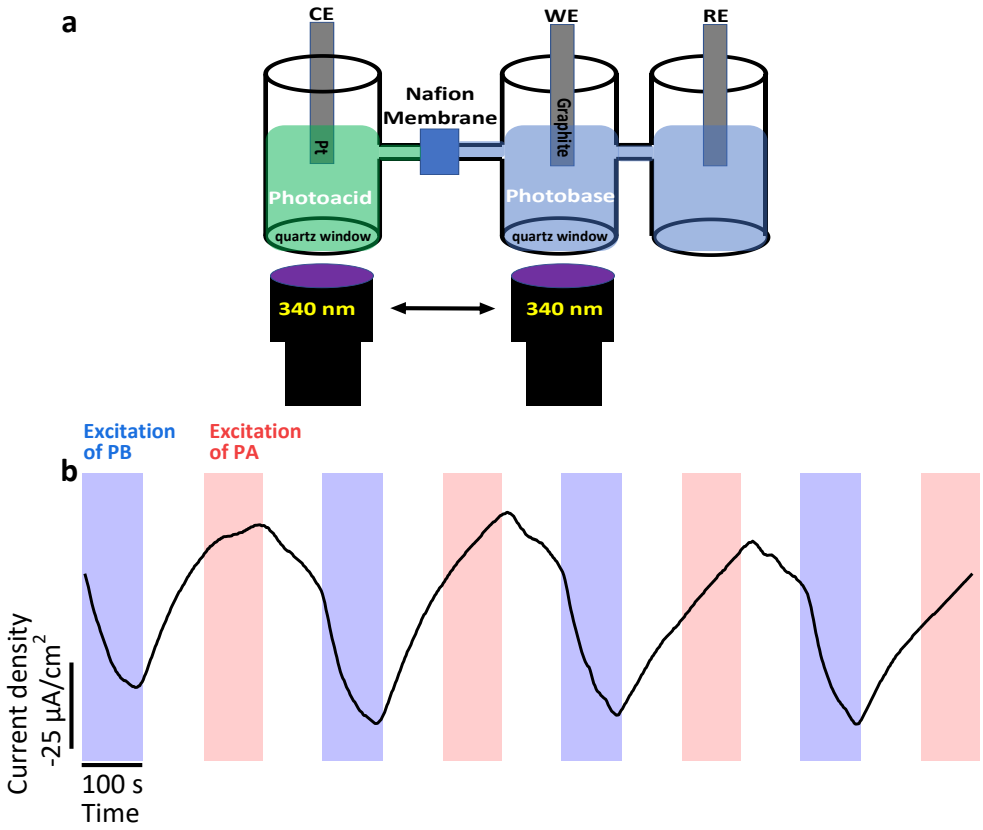

Figure 7. H-cell setup. Photocurrent control by alternate irradiation of 6AQ (PB) and 2N6S (PA). **a**. A schematic representation of the H-cell along with other components of the setup. **b**. Changes in current upon alternate irradiation of 6AQ and 2N6S at the bias of -1V.

Light-induced proton pumping between the two half cells

Following observing that the photocurrent response and polarity can be regulated in the H-cell electrochemical setup by irradiating the PA or the PB, in the last section of our study, we wish to explore the role of the proton-pumping between the two half cells. To do so, we have used the discussed H-cell with the separated Nafion membrane, but now, without the electrodes, while having the 2N6S PA and 6AQ PB in separate cells. As in all previous cases, upon light irradiating the 2N6S will result in proton dissociation, while irradiation of the 6AQ will result in proton association. One of the challenges in using Brønsted PA and PB is the competition with the proton recombination process, meaning the immediate return of the proton to the PA or the deprotonation of the PB upon returning to their ground state. In some cases, other processes can influence this recombination, such as proton transfer to/from another proton acceptor/donor that is not water. In our study, the participation of the formed ions (RO^- /H^+/RNH^+) in the electrochemical process competes with fast recombination. In this section, in the absence of the electrochemical setup, we are targeting the ability of the Nafion membrane to capture and pump protons from one half-cell to the other, which also competes with the recombination process. To explore this, we have used the H-cell discussed above while measuring the concentration of protons, i.e., the pH of the solution, in each half-cell upon a similar cycle of irradiation as above (**Figure 8**). While placing the pH electrode in the half-cell containing the 6AQ PB, a pH increase was measured upon irradiation of 2N6S that continued also in dark, while only upon irradiation of the 6AQ, a decrease in the pH was observed that also continued in the dark until the start of the next cycle (**Figure 8a**). The opposite trend was obtained while placing the pH electrode in the half-cell containing the 2N6S PA, where the pH was decreased upon irradiation of 2N6S and continued to decrease in dark while upon irradiation of 6AQ, the pH was increased and continued to increase in dark (**Figure 8b**). The mirror image of the two independent experiments indicates a proton transport through the Nafion membrane of the H-cell, resulting in a light-induced modulation of the pH by switching the irradiation between 2N6S and 6AQ.

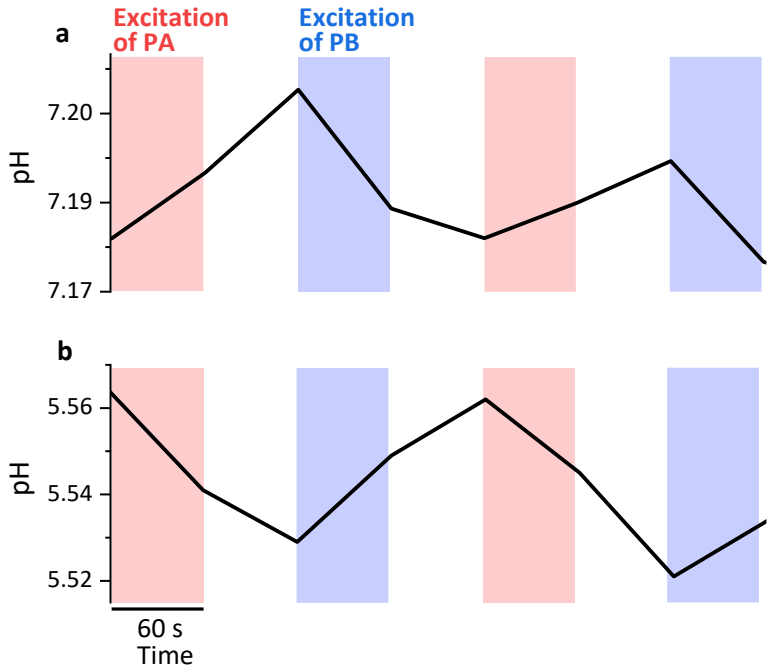

Figure 8. Irradiation of 2N6S and 6AQ triggers proton pumping in the electrochemical cell. pH changes were monitored in the (**a**) photobase and (**b**) photoacid compartments upon alternate irradiation of photoacid and photobase with no electrochemical setup.

Conclusions

In this study, we show the potential of using PAs (2N6S) and PBs (6AQ) in a photoelectrochemical setup for light-controlled current generation. By using several electrochemical techniques (CV and CA) acquired before and during the irradiation of the solution in both single-cell and two-compartment H-cell configurations, we observed photocurrent generation and discussed the role of ESPT from/to the PA/PB in the process. Our results indicate that the formed ions in the excited state ($RO^-/H^+/RNH^+$) have a crucial role in the electron transfer processes involving the WE and CE in both the negative and positive bias regimes. By using a methylated derivative of a photoacid that cannot undergo the ESPT process, we validated that the observed photocurrent generation is not due to the direct sensitization of the electrode by the excited PA. The H-cell configuration allowed photo-modulate the electrical current intensity and polarity by irradiating a specific half-cell, either the one of the PB or the one of the PA, while the proton-conducting membrane separating the half cells is in charge of proton pumping between them. Our study here represents a new concept in photoelectrochemistry and shifts the discussion from purely electronic processes to processes involving proton transfer. The concepts initiated in this study can be further utilized

in future devices targeting light-responsive energy production, energy storage, and hydrogen formation applications.

Experimental section

Electrochemical measurements. All electrochemical measurements were conducted using a PalmSens3 potentiostat. The electrolyte solution in all measurements contained 0.1 M NaCl. In the cyclic voltammetry measurements, the scan rate was 0.02 V/s for the 2N6S and 6AQ measurements and 0.035V/s for the HPTS/MPTS measurements. In chronoamperometry measurements, the time interval was set to 2 s, E_{DC} was -1 V for the experiments at negative potential bias, and 0.5 V for the experiments at positive potential bias. The single-cell configuration was based on a screen-printed electrode with a graphite working electrode with a surface area of 0.079 cm^2, platinum counter electrode, and silver coated with silver chloride reference electrode. The concentrations of the photoacids/photobases used in the single-cell configuration were: 0.5 mM for 2N6S and 6AQ and 0.2 mM for HPTS and MPTS. The light irradiation in the single-cell configuration was above the sample using a 340 nm LED with a maximum power output of 60 mW (M340L4, ThorLabs) for the excitation of 2N6S and 6AQ or a 405 nm LED with a maximum power output of 540 mW (M405L4, ThorLabs) for the excitation of HPTS and MPTS. Both LEDs were controlled by a T-cube LED driver (LEDD1B, ThorLabs). The H-cell configuration was based on a home-built glass design with a bottom quartz window. The electrodes in the H-cell configuration were graphite working electrode with a surface area of 0.28 cm^2 and the same counter and reference electrodes as described for the single-cell configuration. The concentration of the photoacids/photobases used in the H-cell configuration was 3 mM for both 2N6S and 6AQ. The light irradiation in the H-cell configuration was below the quartz window using a 340 nm LED with a maximum output power of 130 mW (CUD4AF1B, SETi) with a home-built controller.

UV-Vis and fluorescence spectroscopy. UV-Vis measurements were performed using Cary 60 spectrophotometer (Agilent) and the fluorescence measurements were performed using Fluorolog fluorometer (HORIBA). A quartz cuvette with a pathlength of 0.5 cm was used for both the UV-Vis and fluorescence measurements. The slit size in the fluorescence measurements was adjusted to 2 nm. The concentration of photoacids/photobases used in the spectroscopy measurements was 0.1mM.

Acknowledgments

A.Y. is supported by the Ariane de Rothschild Fellowship. Y.S. is supported by fellowships of the Nancy & Stephen Grand Technion Energy Program (GTEP) and by a Schulich Graduate fellowship. N.Am. thanks the US-Israel Binational Science Foundation (number 2018239), and the Ministry of Science and Technology (number 3-16243), for financial support. N.Ad. thanks the "Nevet" grant from GTEP and a Technion VPR Berman Grant for Energy Research. Some of the results reported in this work were obtained using central facilities at the Technion's Hydrogen Technologies Research Laboratory (HTRL) supported by the Nancy & Stephen GTEP, the ADELIS Foundation, and the Solar Fuels I-CORE as well as the Russel Berrie Nanotechnology Institute (RBNI). We thank Dr. Rachel Edrei for technical support.

Conflicts of interest

There are no conflicts to declare.

References

1. Ibrahim, N.; Kamarudin, S. K.; Minggu, L. J., Biofuel from biomass via photo-electrochemical reactions: An overview. *J. Power Sources* **2014,** *259*, 33-42.
2. Li, R., Latest progress in hydrogen production from solar water splitting via photocatalysis, photoelectrochemical, and photovoltaic-photoelectrochemical solutions. *Chinese Journal of Catalysis* **2017,** *38* (1), 5-12.
3. Cheng, W.-H.; de la Calle, A.; Atwater, H. A.; Stechel, E. B.; Xiang, C., Hydrogen from Sunlight and Water: A Side-by-Side Comparison between Photoelectrochemical and Solar Thermochemical Water-Splitting. *ACS Energy Letters* **2021,** *6* (9), 3096-3113.
4. Kavan, L., Electrochemistry and dye-sensitized solar cells. *Current Opinion in Electrochemistry* **2017,** *2* (1), 88-96.
5. Molaeirad, A.; Janfaza, S.; Karimi-Fard, A.; Mahyad, B., Photocurrent generation by adsorption of two main pigments of Halobacterium salinarum on TiO2 nanostructured electrode. *Biotechnol Appl Biochem* **2015,** *62* (1), 121-5.
6. Armendáriz-Mireles, E. N.; Rocha-Rangel, E.; Caballero-Rico, F.; Ramírez-de-León, J. A.; Vázquez, M., Photocurrent generation by dye-sensitized solar cells using natural pigments. *Biotechnol Appl Biochem* **2017,** *64* (1), 143-148.
7. Castillo-Robles, J. A.; Rocha-Rangel, E.; Ramírez-de-León, J. A.; Caballero-Rico, F. C.; Armendáriz-Mireles, E. N., Advances on Dye-Sensitized Solar Cells (DSSCs) Nanostructures and Natural Colorants: A Review. *Journal of Composites Science* **2021,** *5* (11), 288.
8. Ouyang, B.; Wang, Y.; Zhang, R.; Olin, H.; Yang, Y., Dual-polarity output response-based photoelectric devices. *Cell Reports Physical Science* **2021,** *2* (5), 100418.
9. Fu, Y.; Zou, K.; Liu, M.; Zhang, X.; Du, C.; Chen, J., Highly Selective and Sensitive Photoelectrochemical Sensing Platform for VEGF165 Assay Based on the Switching of Photocurrent Polarity of CdS QDs by Porous Cu2O-CuO Flower. *Analytical Chemistry* **2020,** *92* (1), 1189-1196.
10. Gawęda, S.; Podborska, A.; Macyk, W.; Szaciłowski, K., Nanoscale optoelectronic switches and logic devices. *Nanoscale* **2009,** *1* (3), 299-316.

11. Fornaciari, J. C.; Weng, L.-C.; Alia, S. M.; Zhan, C.; Pham, T. A.; Bell, A. T.; Ogitsu, T.; Danilovic, N.; Weber, A. Z., Mechanistic understanding of pH effects on the oxygen evolution reaction. *Electrochim. Acta* **2022,** *405*, 139810.
12. Lamoureux, P. S.; Singh, A. R.; Chan, K., pH Effects on Hydrogen Evolution and Oxidation over Pt(111): Insights from First-Principles. *ACS Catalysis* **2019,** *9* (7), 6194-6201.
13. Goyal, A.; Koper, M. T. M., The Interrelated Effect of Cations and Electrolyte pH on the Hydrogen Evolution Reaction on Gold Electrodes in Alkaline Media. *Angew. Chem. Int. Edit.* **2021,** *60* (24), 13452-13462.
14. Selli, E.; Chiarello, G. L.; Quartarone, E.; Mustarelli, P.; Rossetti, I.; Forni, L., A photocatalytic water splitting device for separate hydrogen and oxygen evolution. *Chemical Communications* **2007,** (47), 5022-5024.
15. Strmcnik, D.; Uchimura, M.; Wang, C.; Subbaraman, R.; Danilovic, N.; van der Vliet, D.; Paulikas, A. P.; Stamenkovic, V. R.; Markovic, N. M., Improving the hydrogen oxidation reaction rate by promotion of hydroxyl adsorption. *Nat. Chem.* **2013,** *5* (4), 300-306.
16. Wang, X.; Xu, C.; Jaroniec, M.; Zheng, Y.; Qiao, S.-Z., Anomalous hydrogen evolution behavior in high-pH environment induced by locally generated hydronium ions. *Nat. Commun.* **2019,** *10* (1), 4876.
17. Govindarajan, N.; Xu, A.; Chan, K., How pH affects electrochemical processes. *Science* **2022,** *375* (6579), 379-380.
18. Arnaut, L. G.; Formosinho, S. J., Excited-state proton transfer reactions I. Fundamentals and intermolecular reactions. *J. Photochem. Photobiol., A* **1993,** *75* (1), 1-20.
19. Pines, E.; Huppert, D.; Gutman, M.; Nachliel, N.; Fishman, M., The pOH jump: determination of deprotonation rates of water by 6-methoxyquinoline and acridine. *J. Phys. Chem.* **1986,** *90* (23), 6366-6370.
20. Driscoll, E. W.; Hunt, J. R.; Dawlaty, J. M., Photobasicity in Quinolines: Origin and Tunability via the Substituents' Hammett Parameters. *J. Phys. Chem. Lett.* **2016,** *7* (11), 2093-2099.
21. Pines, D.; Pines, E., Solvent Assisted Photoacidity. In *Hydrogen-Transfer Reactions*, 2006; pp 377-415.
22. Burnstine-Townley, A.; Mondal, S.; Agam, Y.; Nandi, R.; Amdursky, N., Light-Modulated Cationic and Anionic Transport across Protein Biopolymers**. *Angew. Chem. Int. Edit.* **2021,** *60* (46), 24676-24685.
23. Yucknovsky, A.; Mondal, S.; Burnstine-Townley, A.; Foqara, M.; Amdursky, N., Use of Photoacids and Photobases To Control Dynamic Self-Assembly of Gold Nanoparticles in Aqueous and Nonaqueous Solutions. *Nano Letters* **2019,** *19* (6), 3804-3810.
24. Yucknovsky, A.; Rich, B. B.; Westfried, A.; Pokroy, B.; Amdursky, N., Self-Propulsion of Droplets via Light-Stimuli Rapid Control of Their Surface Tension. *Adv. Mater. Interfaces* **2021,** *8* (22), 2100751.
25. Peretz-Soroka, H.; Pevzner, A.; Davidi, G.; Naddaka, V.; Kwiat, M.; Huppert, D.; Patolsky, F., Manipulating and Monitoring On-Surface Biological Reactions by Light-Triggered Local pH Alterations. *Nano letters* **2015,** *15* (7), 4758-4768.
26. White, W.; Sanborn, C. D.; Reiter, R. S.; Fabian, D. M.; Ardo, S., Observation of Photovoltaic Action from Photoacid-Modified Nafion Due to Light-Driven Ion Transport. *Journal of the American Chemical Society* **2017,** *139* (34), 11726-11733.
27. Haghighat, S.; Ostresh, S.; Dawlaty, J. M., Controlling Proton Conductivity with Light: A Scheme Based on Photoacid Doping of Materials. *J. Phys. Chem. B* **2016,** *120* (5), 1002-1007.

28. White, W.; Sanborn, C. D.; Fabian, D. M.; Ardo, S., Conversion of Visible Light into Ionic Power Using Photoacid-Dye-Sensitized Bipolar Ion-Exchange Membranes. *Joule* **2018,** *2* (1), 94-109.
29. Wang, L.; Wen, Q.; Jia, P.; Jia, M.; Lu, D.; Sun, X.; Jiang, L.; Guo, W., Light-Driven Active Proton Transport through Photoacid- and Photobase-Doped Janus Graphene Oxide Membranes. *Adv. Mater.* **2019,** *31* (36), 1903029.

Supplementary Information

Switching of photocurrent polarity in electrochemical cells with light via an excited state proton transfer mechanism

Anna Yuchnovsky[1,a], Yaniv Shlosberg[1,2a], Noam Adir[1,2], and Nadav Amdursky[1,2*]

[1] Schulich Faculty of Chemistry, Technion, Haifa 32000, Israel

[2] Grand Technion Energy Program, Technion, Haifa 32000, Israel

[a] Equal contribution

*Corresponding author: amdursky@technion.ac.il

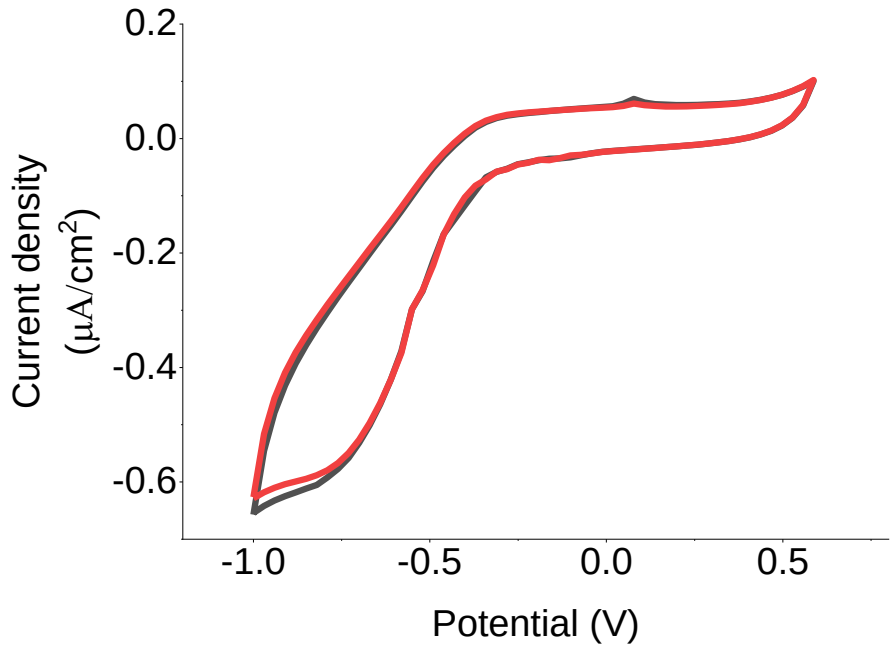

Figure S1. CV of electrolyte in dark (black) and light (red).

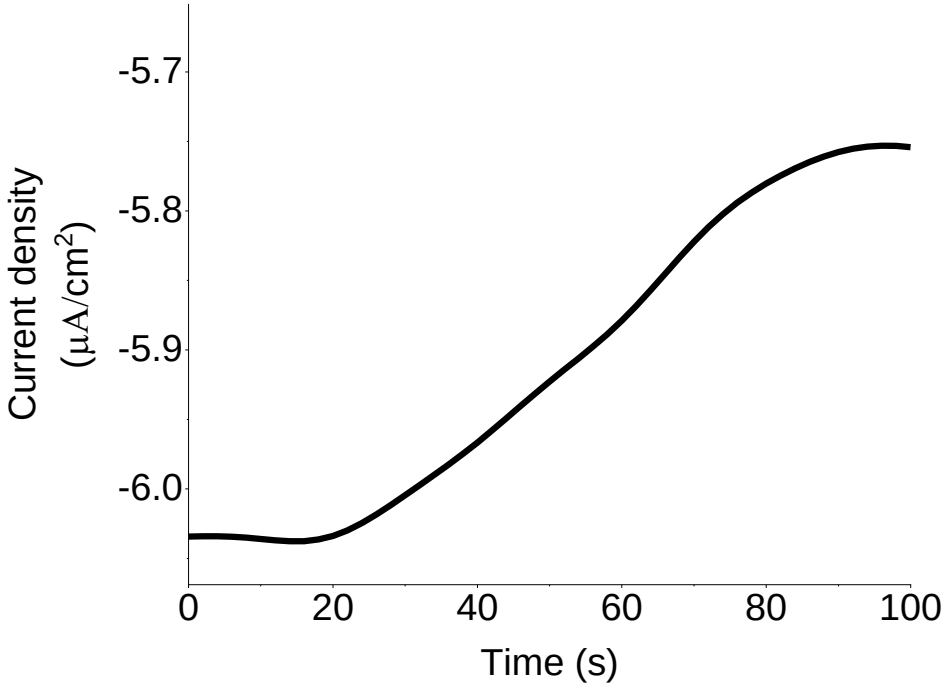

Figure S2. CA of a 60 µL electrolyte drop with addition of 1 µL HCl on top of the drop. The HCl was added at time = 0 s. The measurement was conducted at applied potential bias of -1 V on the WE.

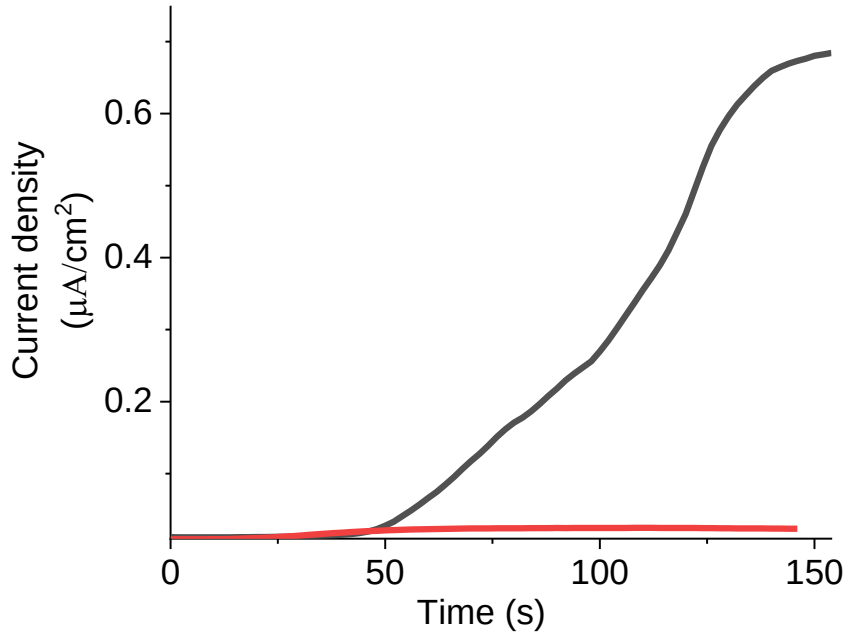

Figure S3. CA of a 60 µL electrolyte drop with addition of 2.5 µL PA solution at pH 13 (black line) or 2.5 µL 0.1M NaOH solution (red line). After the addition of 2.5 µL PA to 60 µL electrolyte, the resulting solution pH is >11, so the dominant form of PA is RO^-. Both solutions were added at time = 0 s. The measurement was conducted at applied potential bias of 0.5 V on the WE.

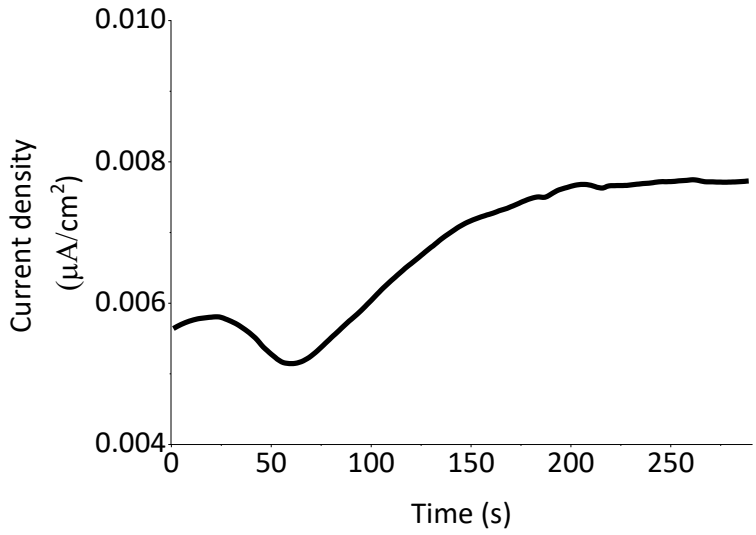

Figure S4. CA of a 60 µL electrolyte drop with addition of 1 µL HCl on top of the drop. The HCl was added at time = 0 s. The measurement was conducted at applied potential bias of 0.5 V on the WE.

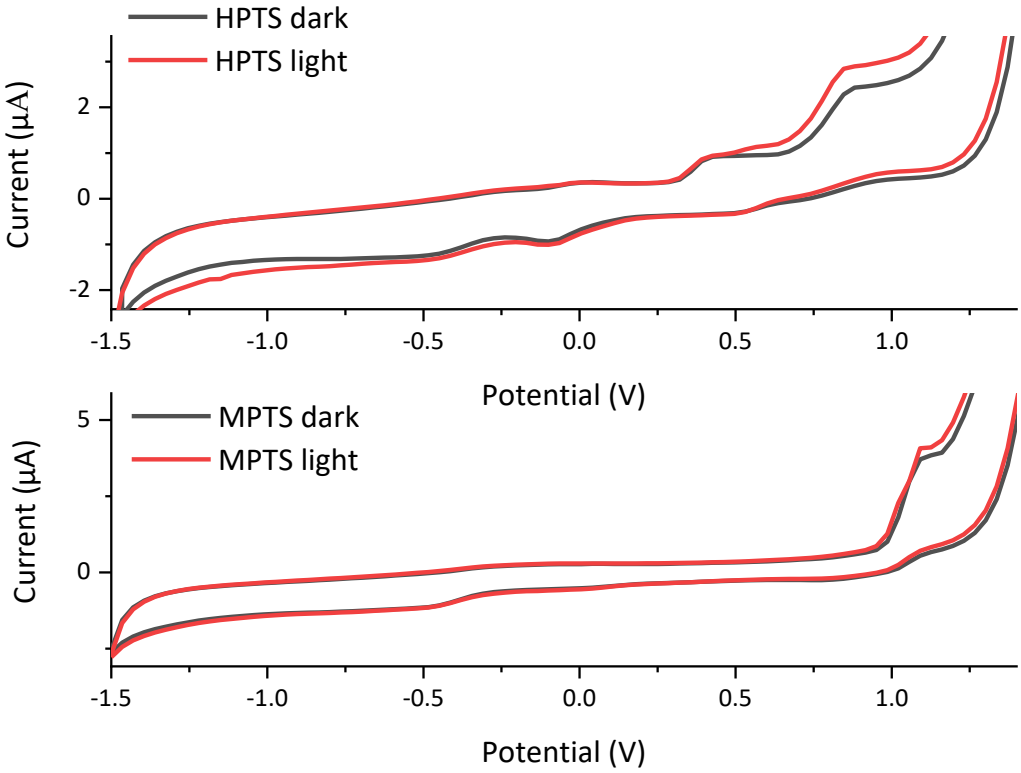

Figure S5. CV measurement of HPTS (top) and MPTS (bottom) in dark and upon light irradiation (λ_{ex}=405 nm).

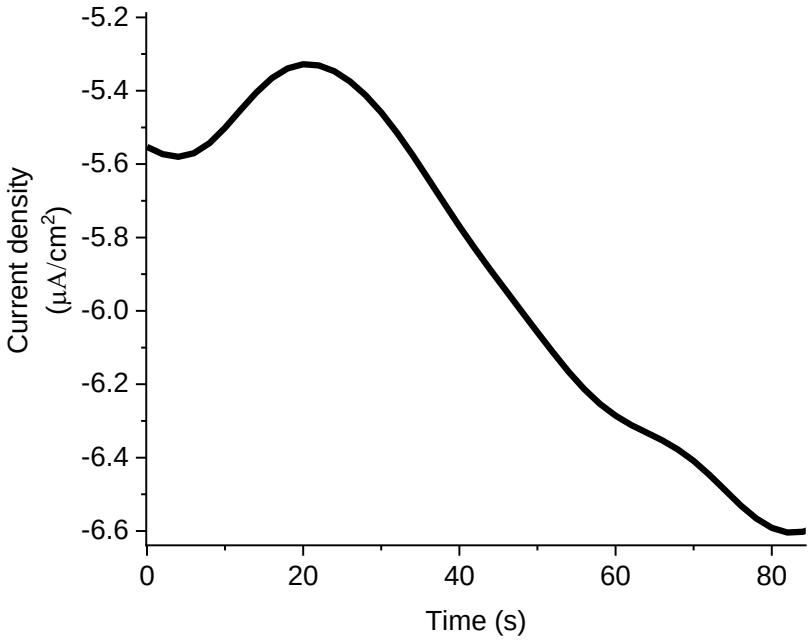

Figure S6. CA of a 60 µL electrolyte drop with addition of 2.5 µL PB solution at pH 2. After the addition of 2.5 µL PB to 60 µL electrolyte, the resulting solution pH is ~ 3.4, so the dominant form of PB is RNH^+. The PB was added at time = 0 s. The measurement was conducted at applied potential bias of -1 V on the WE.

Table S1. Photocurrent reaction lifetime (τ) at the negative bias regime (-1V) obtained from the plots in Figures 3a, 6a and 7b using a single-exponential fitting of the decay or growth components.

2N6S		**6AQ**	
One-cell	**H-cell**	**One-cell**	**H-cell**
9.6±1 s	89.8±9 s	47.5±3 s	45.6±2 s